



Seismic vulnerability assessment of masonry building supported by STRP isolators

Md Basir Zisan^{1,2} · Md. Naimul Haque³ · Md. Abul Hasan⁴

Received: 2 June 2022 / Accepted: 10 August 2022 / Published online: 23 August 2022
© The Author(s), under exclusive licence to Springer Nature Switzerland AG 2022

Abstract

Scrap tire rubber pad (STRP) isolators are made from scrap automobile tires, which are expected to be a low-cost material for earthquake-resistant design of low-to-medium-rise buildings in developing countries. This paper describes the seismic vulnerability of a unbonded STRP (U-STRP) base-isolated masonry building using the finite element method. The three-dimensional model of the U-STRP isolators is placed between the foundation and the building without any bonding between them. As a result, the inertia force of the building is transferred to the foundation through the friction. Two alternative versions of the U-STRP isolator: strip-shaped and square-shaped, are analyzed, which have comparable geometric and stiffness properties. The fidelity of the U-STRP isolator model is confirmed using the numerical analysis and experimental results. The seismic vulnerability of the masonry base-isolated building is determined using the pushover analysis and the fragility curves and then compared to that of the identical fixed-base building. The findings show that masonry buildings with uniformly distributed square-shaped U-STRP isolators suffer low damage and base shear compared to those of the same size of strip-shaped U-STRP isolators. The U-STRP base-isolated masonry building has superior seismic performance to that of an identical fixed-base building, and a square-shaped U-STRP is more effective than the strip-shaped isolator.

Keywords U-STRP · Fragility curves · Pushover analysis · Seismic vulnerability · Masonry building · Low-cost isolator

Introduction

Masonry building is a widespread construction method due to its cost-effectiveness and ease of construction. The number of unreinforced buildings, including residential houses, educational facilities, government offices, and historic structures, is significant, especially in southern Asia. Most of these structures are built using traditional methods without any seismic provisions. The lateral load capacity of a masonry building is low due to its inadequate tensile

strength and low ductility (Feng et al., 2011; Murtyl et al., 2004). These buildings are seismically vulnerable due to poor mortar connections, wall openings, improper wall sections and dimensions, and lack of vertical confinement. The lateral load capacity of existing or new masonry constructions can be increased by utilizing seismic protection techniques (Choudhury et al., 2015; Milani et al., 2017, 2018; Murtyl et al., 2004). For this purpose, strengthening-based retrofitting methods are commonly utilized. Seismic base isolation, which is utilized to reduce seismic demand by lengthening the natural period, is also an alternative strategy. Despite being acknowledged as a promising technology, base isolation is rarely used in conventional and brick structures due to high cost, weight, and unavailability, particularly in developing countries (Kelly, 2002; May, 2002; Pan et al., 2005). As a result, cost savings and the simple design concept of the base isolator are important considerations.

For low-to-medium-rise buildings, several low-cost base-isolations such as friction interfaces or sliding interfaces composed of marble, graphite powder, screened gravel, rubber-sand, and paraffin wax between structure and foundation have been proposed (Li, 1984; Nanda et al., 2015;

✉ Md Basir Zisan
basirzisan@cuet.ac.bd

¹ Department of Civil Engineering, Chittagong University of Engineering and Technology, Chattogram 4349, Bangladesh

² Kyoto University, Kyoto 615-8540, Japan

³ Department of Civil Engineering, East West University, Aftabnagar, Dhaka 1212, Bangladesh

⁴ Department of Disaster Engineering and Management, Chittagong University of Engineering and Technology, Chattogram 4349, Bangladesh

Qamaruddin et al., 1986). The scrap tire pad (STP) isolator, which is made by stacking STP one above another without adhesive, was proposed by Turer and Özden (2008). But the application of unbonded layers of STP is impractical. A discarded Kart tire filled with recycled elastomeric materials and aggregates was proposed by Hadad et al. (2017). It has the potential to improve seismic performance. Further research is needed on fire resistance, the effects of ambient conditions, tire dimensions, and the size and amount of filling grains on dynamic response. A recycled tire bearing (RTB) was studied by Morales et al. (2018). It consists of tires that have been cut through their diameter and inserted between the structural slab of a designated room and a service floor surface. The vertical vibration, rocking motion, and pre-compression force are described as significant challenges for this system.

The scrap tire rubber pad (STRP) isolator is an attractive and low-cost alternative to SREI or FREI applicable for ordinary structures, as proposed by Mishra (2012). It is made by bonding several tire pads stacked one above another. A STRP isolator can be used without the thick endplates that are necessary to fasten the isolator to the structural base in the case of SREI. As a result, the cost of the isolator is significantly reduced. An isolator which is utilized without any bonding is known as an unbonded STRP (U-STRP). This type of isolator transfers the inertia force through friction. Since there are no difficulties relating to mechanical fastening, this type of isolator can be used in existing structures as well. In the case of an existing structure, the lifting of the superstructure method can be used to install the U-STRP isolator without interfering with serviceability. The feasibility of an unbonded STRP isolator has been studied by Mishra (2012) and Zisan and Igarashi (2021). It shows that the stiffness of the U-STRP isolator degrades with lateral displacement due to roll-over deformation, which reduces the seismic demands of supporting structures. Again, the U-STRP isolator exhibits stiffness hardening at large deformation when the vertical edges of the isolator touch the structural elements during roll-over deformation as shown

in Fig. 1. This isolator is stable until the roll-over deformation reaches 250% shear displacement (Zisan and Igarashi, 2021). This feature is unavailable in the conventional SREI or bonded isolator. This feature is advantageous in limiting the shear displacement during a maximum earthquake event (Van Engelen et al., 2016). Some of the tire-derived base-isolators have already been tested for seismic isolation of frame structures. A recycled rubber-fiber reinforced bearing (RR-FRB) made with recycled tire chips, carbon, and polyester fibers exhibits more advantages than that of SREI or FREI in terms of dissipation capacity, manufacturing cost, and weight (Spizzuoco et al., 2014). Shaking table tests (Calabrese et al., 2015; Maddaloni et al., 2017; Losanno et al., 2019) reveal significant improvement in isolated structures and an excellent re-centering capability of RR-FRBs. The drawback is the low shear strain and tensile capacity.

Mishra et al. (2012), Mishra and Igarashi (2013) and Mishra et al. (2013) examined the stiffness and damping of U-STRP isolators as well as the hyperelastic properties of scrap tires. It was claimed that the U-STRP isolator has damping ratios of 10–22% and vertical-to-horizontal stiffness ratios of 450–600, above 150, which are critical for isolation material (Eurocode 8, 2004). A pseudo-dynamic test of the U-STRP isolator (Mishra et al., 2014) and a numerical analysis of a three-story STRP base-isolated building indicate that the STRP isolator is feasible for low-to-medium-rise buildings. The numerical analysis ignored the friction-based unbonded boundary condition of the U-STRP isolator and also the softening and hardening characteristics. Later, Zisan and Igarashi (2021) investigated the lateral performance and deformation capacity of unbonded square and strip-shaped U-STRP isolators. These studies covered the influence of the length-to-width ratio and bearing height on the horizontal stiffness, damping, and seismic demand. It also provides a theoretical formulation for the lateral stiffness of U-STRP isolators. To judge the effectiveness of the U-STRP isolator in a real building, it is necessary to assess the performance of a U-STRP base-isolated building in real-time conditions. Therefore, the objective of this paper is to analyze

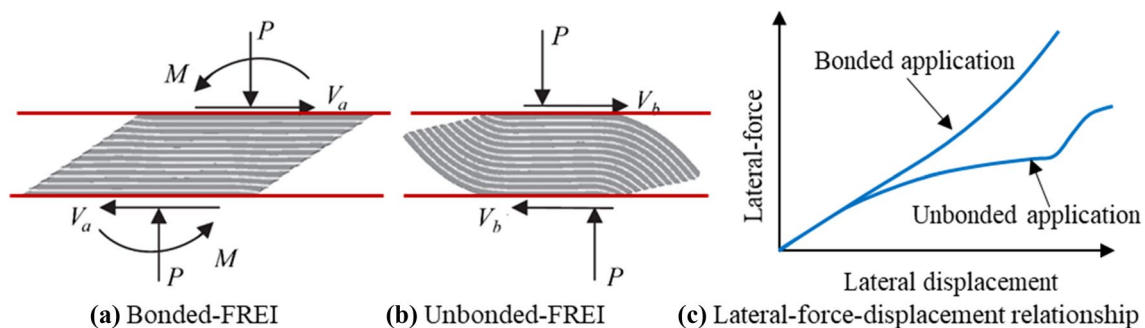


Fig. 1 Lateral deformation and force–displacement relationship of bonded and unbonded STRP isolators

the seismic vulnerability of masonry buildings resting on a three-dimensional model of U-STRP isolators. Both square-shaped and strip-shaped isolators having the same stiffness properties are taken into consideration. Pushover and fragility analyses are performed in order to assess the performance and vulnerability of the base-isolated building.

FE modelling of masonry building

Figure 2 shows a two-story masonry building with a plan dimension of 15 m × 10 m, typically found in the rural areas of Bangladesh. The overall height of the building above the grade beam is 6260 mm, and the story height is 3130 mm. All brick columns are equally spaced by 5000 mm in the *X* (strong axis) and *Y* (weak axis) directions. The principal components of the building are the reinforced concrete floor, grade beam, and load-bearing brick wall. The brick-made grade beams are 390 × 600 mm in size, and U-STRP isolators are placed below the grade beams. All the brick columns are 390 × 390 mm in size, and the brick walls and the concrete slab are 130 mm. Openings for doors and windows are 1100 × 2200 mm and 1400 × 1400 mm, respectively. To

check the premature damage of walls, a reinforced concrete lintel of size 100 × 200 mm is inserted on top of wall openings. The unit weight of concrete and that of the brickworks is assumed to be 2400 kg/m³ and 1950 kg/m³, respectively.

The material parameters for the masonry units are taken from Choudhury et al. (2015) and those for the reinforced concrete are found in Jain and Kennedy (1974) and Crisfield (1982). These parameters are listed in Table 1. Isotropic nonlinear material that exhibits cracking in both tension and compression is used for masonry units through a simplified

Table 1 Properties of concrete and masonry units utilized in the FE model

Parameters	Concrete	Masonry
Elastic modulus (GPa)	28.96	1.227
Poisson ratio	0.20	0.15
Yield strength (MPa)	31.6	1.8
Ultimate tensile strength (MPa)	2	0.15
Softening modulus (GPa)	3.62	0.123
Shear retention	0.5	0.5
Angle of friction	30°	30°

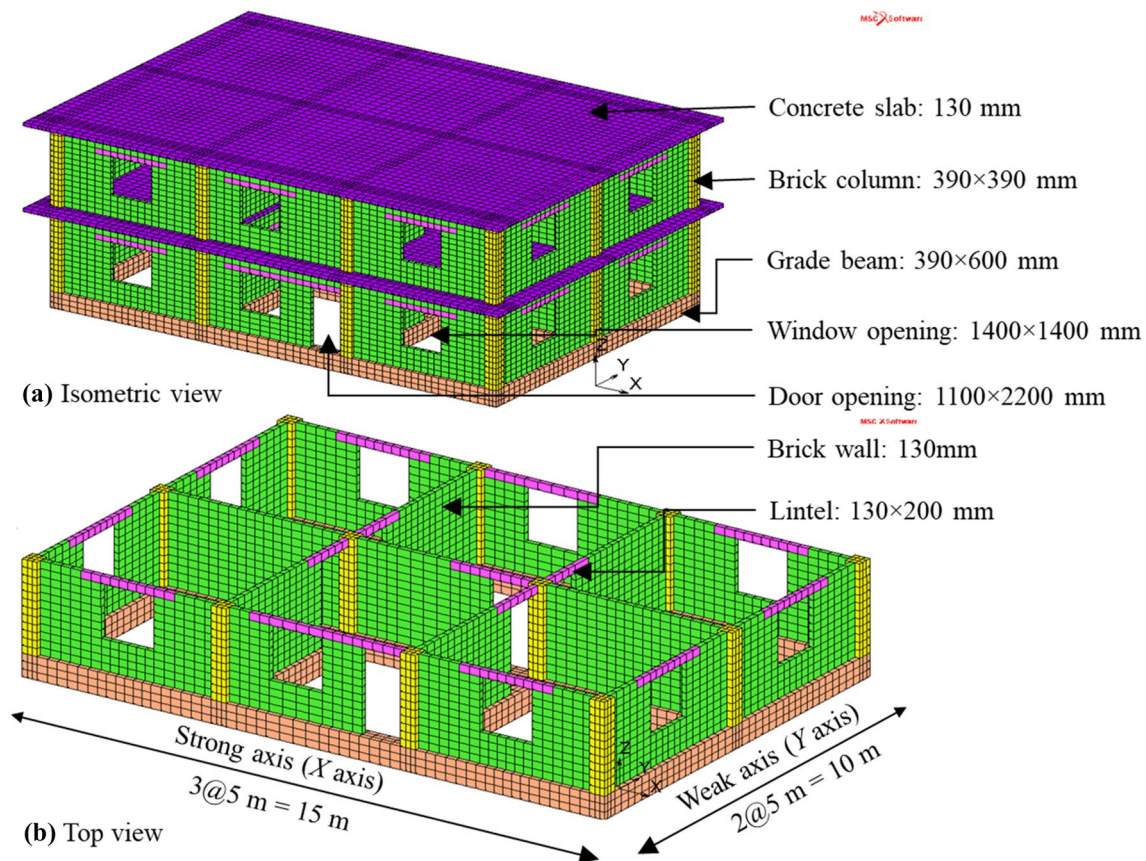


Fig. 2 FE model of masonry building considered in this study

stress–strain relationship, which is shown in Fig. 3 (Choudhury et al., 2015; Habieb et al., 2017). In the figure, f_y and f_u are the yield and ultimate compressive strength of a masonry wall, respectively. The symbol f_t is used to indicate the tensile strength. The stress–strain in tension is linearly elastic until cracking occurs, followed by a softening branch, which indicates micro-crack propagation in the material. The behavior of the masonry unit in compression is linearly elastic until 1.8 MPa, followed by a 2.4 MPa crushing stress and a linear softening branch. The reinforced concrete elements are assumed to behave elastically. This assumption is quite reasonable since the strength of concrete is greater than that of the mortar. The yield strength for concrete is 31.6 MPa. The cracking behavior of mortar primarily determines the overall damage of a masonry structure since its tension capacity is deficient. The peak tensile strength of concrete and that of mortar is 2.0 MPa and 0.15 MPa. These values comply with the experimental data available in the literature and codes of practice. The tension softening modulus is 3.62 GPa and 0.123 GPa for concrete and mortar, respectively, around one-tenth of the elastic modulus. Both concrete and masonry units are modeled using an eight-node, isoparametric, arbitrary hexahedral element.

The maximum strength in tension and compression is calculated using the Mohr–Coulomb yield criterion under plane stress conditions. The yield surface is based on the generalized Mohr–Coulomb model, which was developed by Drucker and Prager. It can be mathematically expressed by (MSC Marc, 2020):

$$f = \alpha J_1 + J_2^{1/2} - \frac{\bar{\sigma}}{\sqrt{3}}, \tag{1}$$

where $\bar{\sigma}$ is the deviatoric stress and α is the material constant. J_1 and J_2 are the 1st and 2nd invariants of the deviatoric stress tensors given below.

$$J_1 = \sigma_{ij} \tag{2}$$

$$J_2 = \frac{1}{2} \sigma_{ij}^d \sigma_{ij}^d \tag{3}$$

The isotropic hardening rule is assumed using the Drucker and Prager model, described as follows:

$$c = \frac{\sigma}{[3(1 - 12\alpha^2)]^{1/2}} \text{ and } \sin\phi = \frac{3\alpha}{(1 - 12\alpha^2)^{1/2}}, \tag{4}$$

where c is the cohesion and ϕ is the angle of friction. In the current study, the cohesion and the angle of friction are assumed to be 0.15 MPa and 30°, respectively (Choudhury et al., 2015; Habieb et al., 2017).

Figures 4 and 5 show the natural period and mode shapes of the fixed-base and base-isolated masonry buildings. The first mode period of the fixed-base building is 0.15 s, which is comparable to the period of a low-rise masonry building estimated by the flowing equation (Calvi, 1999).

$$T = 0.04h^{3/4} \tag{5}$$

Here, h is the total height of the building in meters, and period T is in seconds. In comparison with the fixed-base building, Table 2 indicates that the period of the STRP base-isolated building is substantially higher than that of the fixed-base building. The first and second modes of the building are translational modes. The third mode is rotation, whereas the fourth one is the combined mode. In base-isolated buildings, the first mode is the largest model in which the STRP isolator is subjected to large displacement.

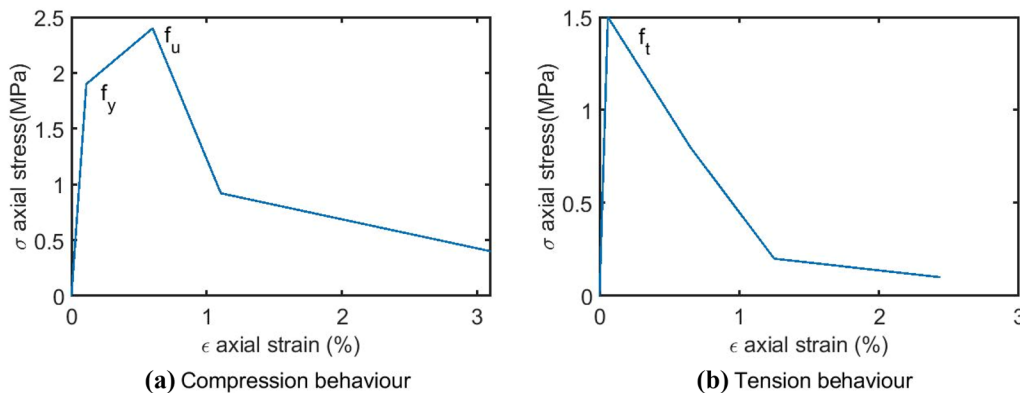


Fig. 3 Simplified nonlinear behavior of masonry units in compression and tension

Fig. 4 Period and mode shapes of fixed-base masonry buildings

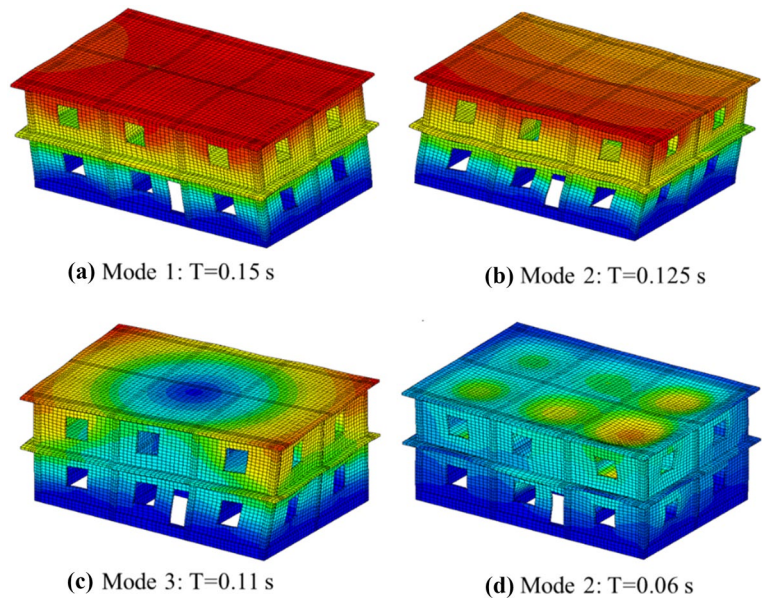


Fig. 5 Period and mode shapes of DBI masonry buildings

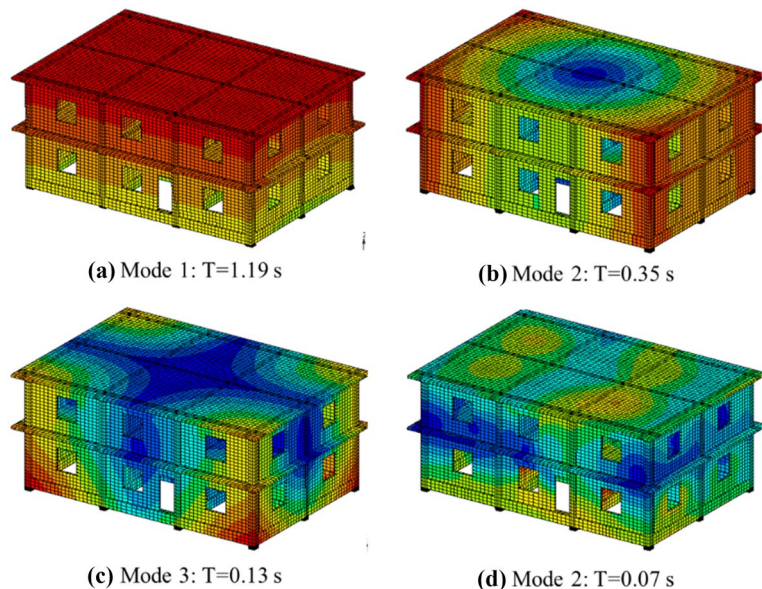


Table 2 Period of fixed base, DBI and SBI buildings

	1st mode	2nd mode	3rd mode	4th mode
Fixed-base	0.15	0.125	0.11	0.06
DBI system	1.19	0.48	0.13	0.07
SBI system	1.08	0.41	0.12	0.06

FE modelling of U-STRP isolators

The total mass of the masonry building is 3011 kN. The mass of the isolator is negligible and disregarded. The

size of the isolator is determined based on the pressure on the isolator and the aspect ratio of the isolator. Though AASHTO-LRFD recommends a minimum aspect ratio of 3.0 for bonded isolators, Zisan and Igarashi (2021) recommend an aspect ratio of 3.0 for U-STRP. A minimum aspect ratio is assumed to be 2.50 to keep the pressure on the isolator greater than 2.0 MPa. Figure 6 illustrates the hysteresis loops of U-STRP of size 180 mm × 180 mm × 72 mm under 1.5 MPa and 2.20 MPa compressions, respectively. The horizontal axis represents the elastomer strain (u/t_r), in which u is the displacement of the isolator and t_r is the total rubber thickness. It shows that the U-STRP isolator experiences no sliding until 200% shear displacement.

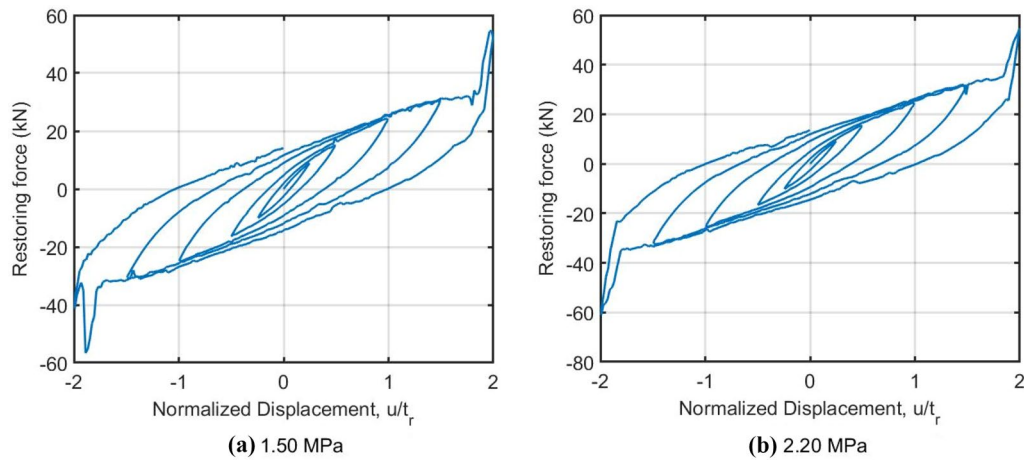
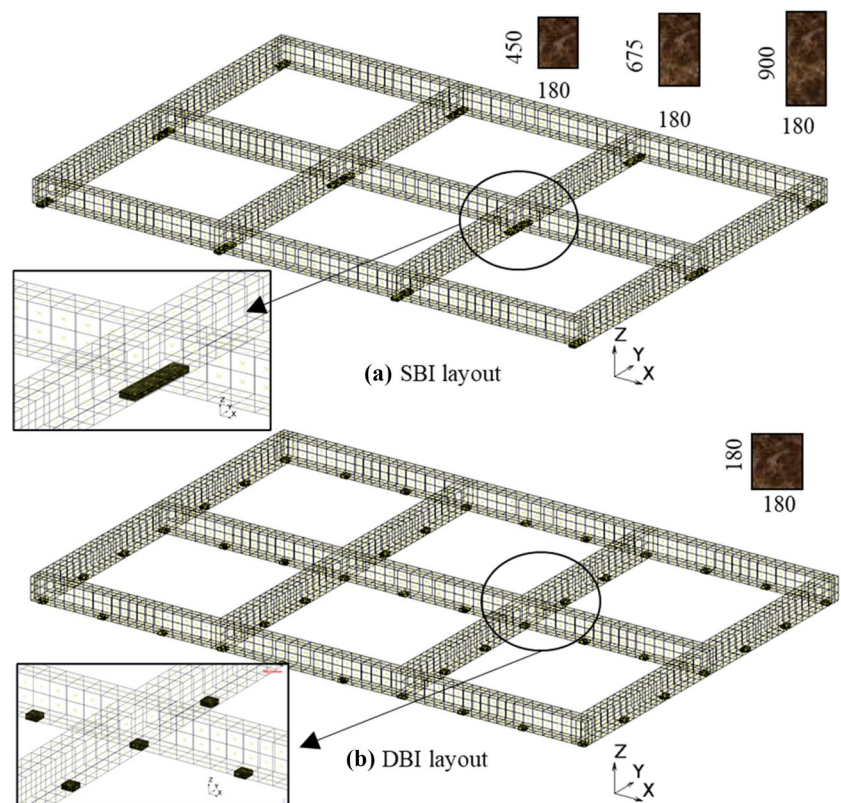


Fig. 6 Force–displacement relationship of $180 \times 180 \times 72$ mm U-STRP isolator

Since there is no rigid foundation in masonry buildings, large strip-shaped and uniformly distributed square-shaped U-STRP isolators are employed. The strip-shaped isolation is termed as SBI, whereas the uniformly distributed square-shaped isolator is named as DBI system. Figure 7 demonstrates the layout of isolators in the SBI and DBI systems, including the size of isolators. In the SBI layout, corner isolators are 450×180 mm, isolators at the periphery and middle position are 675×180 mm, and two

inside isolators are 900×180 mm. In the DBI layout, 36 isolators equally spaced in both X and Y directions have a dimension of 180×180 mm. The minimum aspect ratio of these isolators is 2.50, and the height is 72 mm. The average pressure on isolators in SBI and DBI layouts is 2.18 MPa and 2.02 MPa, respectively. These pressures are substantially below 5.0 MPa, acceptable for 200% shear displacement without exceeding tension $2G \sim 3G$. Here, G is the shear modulus of tire material. The shear modulus of

Fig. 7 Different layout of U-STRP isolator for masonry building (mm)



U-STRP isolators subjected to 3.3–10 MPa compression and 100% shear strain is 0.48–0.75 MPa (Mishra et al., 2014), and the effective damping ratio is 12–16%. The shear modulus at 100% shear and 3.00 MPa working stress is 0.60 MPa. The total area of SBI and DBI isolators is $1377 \times 103 \text{ mm}^2$ and $1361 \times 103 \text{ mm}^2$, respectively. Utilizing a 72 mm thick isolator, the stiffness and period of the masonry building with SBI and DBI systems are about 13.6 kN/mm and 0.95 s, respectively. The lateral stiffness of $180 \times 180 \times 72 \text{ mm}$ size isolator calculated from Fig. 6b is 646, 544, 422, 360, and 600 N/mm at 25%, 50%, 100%, 150%, and 200%, respectively. The stiffness and period of the SBI and DBI systems calculated from the minimum stiffness of $180 \times 180 \times 72 \text{ mm}$ isolator are 15.12 kN/mm and 0.90 s. This period is substantially longer than the period of a fixed base masonry building and close to the finite element analysis results.

Contact modeling

The base-isolated building is rested on a rigid plane called the bottom plane. It can move horizontally in the direction of applied displacement or be fixed in position in a static condition. This rigid plane does not undergo any deformation nor carry any stress and is modeled as a load control element. The control node is defined at the center of the plane, subjected to ground acceleration in dynamic analysis or fixed boundary conditions in static analysis. Touch contact is assumed among isolators, grade beams, and the rigid plane. The friction coefficient, contact algorithm, and contact procedure are the same as described in Zisan and Igarashi (2021). The node-to-segment contact algorithm is utilized in the computation of contact force. The so-called mixed-method based on Herrmann's formulation is used for the large-strain analysis of incompressible rubber. The geometric nonlinearities are included using the updated Lagrangian formulation. The single-step Houbolt operator, a default implicit method used by Marc-Mentat, is used for integration. The Single-Step Houbolt operator $\gamma_1 = 1.5$ and $\gamma = -0.5$ is assumed. The Newton–Raphson iteration with a

relative force and displacement tolerance equal to 0.1 N and 0.1 mm, respectively, is used.

FE model verification

The STRP-4/1 isolator, which has four layers of STRP and a length-to-width ratio of 1.0, has been used in the experiment and FE model verification. The details of the STRP-4/1 isolator and experiment conditions can be found in Mishra (2012). Table 3 shows the comparison of stiffness values of the STRP-4/1 isolator obtained from the past loading test, FE analysis, and an analytical solution (Zisan and Igarashi,). The vertical stiffness, K_v , and the compression modulus E_c are found from the pressure solution approach (Tsai & Kelly, 2002) as follows:

$$K_v = \frac{E_c A}{t_r} \quad (6)$$

$$E_c = \frac{12G_e S^2}{(aa)^2} \left(1 - \frac{\tanh(\alpha a)}{\alpha a} \right) \text{ and } \alpha = \sqrt{\frac{12G_e(1 - \nu_f^2)}{E_f t_f t_{ri}}}, \quad (7)$$

where α denotes the degree of reinforcement flexibility. E_f and t_f are the elastic modulus and equivalent thickness of steel cord, respectively, and t_{ri} is the thickness of the elastomer layer. Figure 8a demonstrates that the lateral force–displacement relationship derived from the FE analysis and that from the experiment are in good agreement. Table 3 shows that the stiffness at various displacement levels obtained by FE analysis has good agreement with the experimental and analytical results. Figure 8b displays the vertical load–displacement relationship in which the vertical stiffness is defined by the slope of the cyclic loading component. The vertical stiffness of the STRP-4/1 isolator matched well with the analytical solution but was significantly overestimated as compared to the test findings. The vertical stiffness in real specimens is reduced since the FE model overlooked the sliding and twisting effects of steel cables (Costello, 1997). The vertical stiffness of the STRP specimen is also affected by the curvature caused by the roundness of tires.

Table 3 Horizontal and vertical stiffness: experimental, FE analysis, and analytical solution

Isolator	Shear strain (%)	Horizontal stiffness, K_h (kN/m)			Vertical stiffness K_v (MN/m)				
		Experiment	FEA	Analytical	Experiment/FEA	FEA/analytical	Experiment	FEA	Analytical
STRP-4/1	37.5	262	258	263.7	1.02	0.98	56.41	79.7	80.0
	75	206	190	188.0	1.08	1.01			
	112.5	163	163	138.0	1.00	1.18			
	150	133	137	120.0	0.97	1.14			

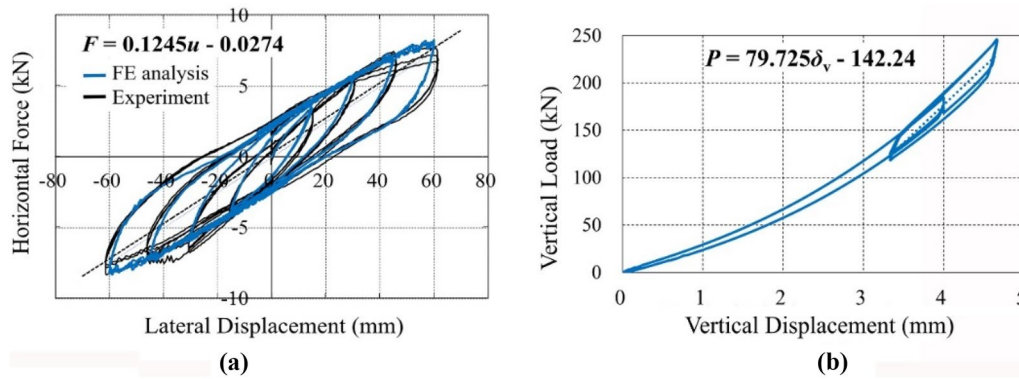


Fig. 8 Force–displacement relationship of STRP-4/1 **a** lateral load, **b** vertical load

Table 4 Effective damping (β %): experiment and FE analysis

Shear strain (%)	Experiment	FEA	Experiment/ FEA
37.5	13.2	15.3	0.86
75	12.2	16.5	0.74
112.5	14.2	15.8	0.90
150	15.0	16.4	0.91

The vertical stiffness of the STRP specimen can be improved by flattening it by surface treatment and pre-compression during the bonding process. Table 4 demonstrates that the FE analysis-derived effective damping of STRP-4/1 is 16.9% greater than the experimental measurement.

Pushover analysis

The effectiveness of U-STRP base isolation is assessed using the damage state of the masonry building. The damage states for fixed-base buildings and those for U-STRP base-isolated buildings are obtained from pushover analysis. For this purpose, the pushover curve of the analyzed buildings is obtained by plotting base shear with respect to the roof displacement. The lateral displacement of the building

base is assumed in the global X , Y , and 45° -direction. The stiffness of the floors is substantially higher than that of masonry units, so the lateral displacement of the floor nodes is assumed to be the same. The first natural vibration mode is considered in pushover analysis since it provides maximum displacement in the base-isolation in a low-rise base-isolated structure. The inter-story drift obtained from the pushover analysis defines the damage state of the masonry building. Table 5 shows the threshold value of inter-story drift and corresponding damage states introduced by Calvi (1999) and used in this study.

According to Table 5, the states of damage in a masonry building can be classified into no damage, slight damage, moderate damage, extensive damage, and collapse damage. Figure 9 shows the performance level on the pushover curve at different damage levels and inter-story drifts as described in Table 5. Masonry structures do not display a clear elastic limit since the cracking load in masonry buildings is significantly smaller than that of a reinforced concrete structure. Besides, masonry structures follow progressive collapse. Based on these criteria, Calvi (1999) merged the first two damage states into a single one called “no damage” and “slight damage.”

The damage states of U-STRP base-isolated buildings are determined using the same criteria used for fixed-base buildings, as described in Table 5 and Fig. 8. The same methodology for fixed-base building is used by Thuyet et al. (2018).

Table 5 Threshold value for damage state and damage criteria in masonry building (Calvi, 1999)

Damage state	Performance criteria
DS1	No damage, either structural or nonstructural
DS2 (moderate)	The inter-story drift limit is 0.1%. Minor structural damage and/or moderate nonstructural damage; the building can be utilized after the earthquake without significant strengthening and repair of structural elements
DS3 (extensive)	The inter-story drift limit is 0.3%. Significant structural damage and extensive non-structural damage. The building could be used after the earthquake without considerable repair. Still, repair and strengthening are feasible
DS4 (collapse)	The inter-story drift limit is 0.5%. Repairing the building is neither possible nor economically reasonable. The structure will have to be demolished after the earthquake. Beyond this DS, global collapse with danger to human life has to be expected

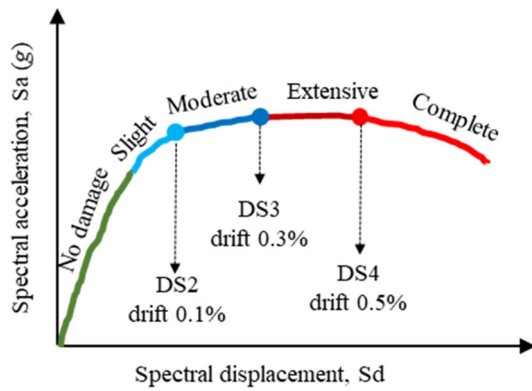


Fig. 9 Performance level on the pushover curve

Thuyet et al. (2018) considered a damaged state, DS5, for damage or instability of the isolator, which is defined by the isolator displacement of 170% shear, the instant of commencement of hardening in an unbonded isolator. A U-STRP isolator exhibits progressive roll-over deformation and no instability until 250% shear strain. However, tension within a U-STRP isolator exceeds $2G \sim 3G$ for displacement exceeding 200% shear, which could be defined as the damage state

of the isolator, DS5. The tension failure of the isolator is ignored in the current study.

Figures 10 and 11 show the contour for the principal value of cracking strain at different damage levels of non-isolated and base-isolated masonry buildings. These damage states are calculated based on the drift ratio within the masonry unit only. It does not consider the strain within the isolator. That is why the contours between fixed-base and base-isolated structures are comparable. The strains that fall outside of the range $[0.003 - 0.003]$ indicate collapse cracking. It shows that the strain is diagonally propagated both in non-isolated and base-isolated buildings. At moderate damage state DS2, strain in the fixed-base building and that of the base-isolated building is within the range $[0.003 - 0.003]$, as shown in Figs. 10a, d, g, and 11a, d, g. In the extensive and collapsed damage states, cracks in the masonry walls that are parallel to the loading directions are significant. These cracks propagate in the diagonal direction and originate from the wall openings. At the collapsed level, horizontal cracks were also generated on the upper floor, especially within the wall perpendicular to the loading direction. At the collapsed state DS4, almost the entire wall of the upper floor experiences a cracking strain larger than 0.003.

Figure 12 shows the pushover curve for fixed-base and base-isolated buildings due to the top floor displacement.

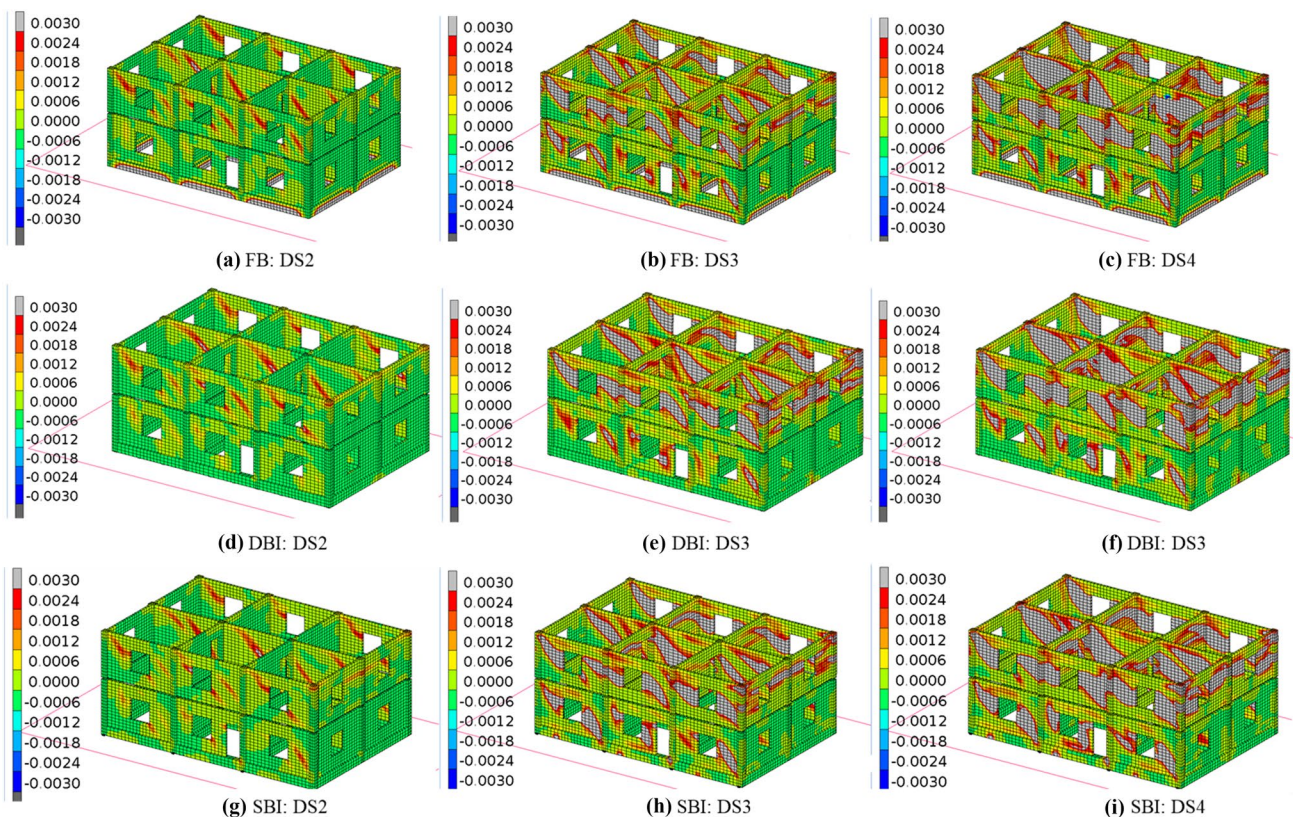


Fig. 10 Cracking contour in different damage states of masonry buildings for displacement in the strong axis

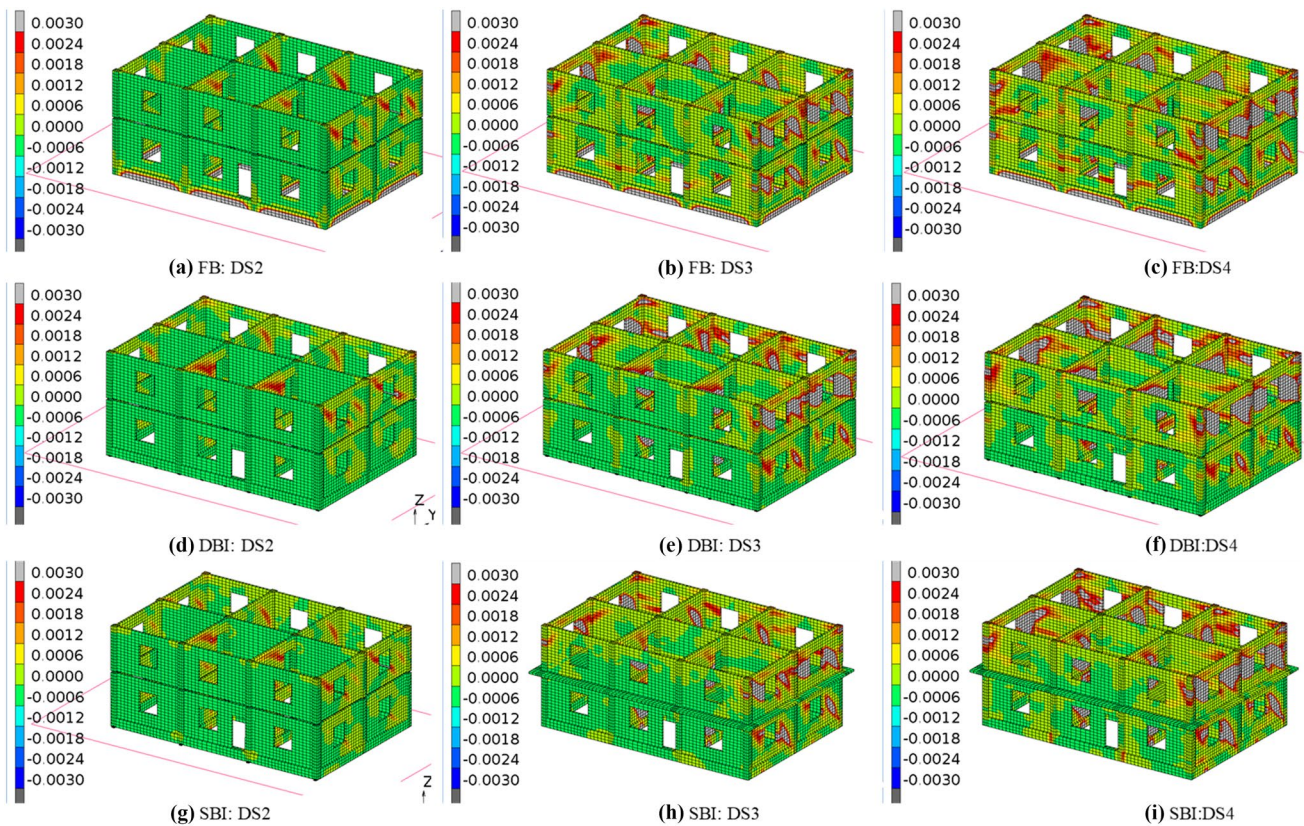


Fig. 11 Cracking contour in different damage states of masonry buildings for displacement in the weak axis

The building is subjected to displacement at the top floor in the strong axis (X), weak axis (Y), and 45° -direction. Floor displacement is applied until failure occurs either within the masonry components or the isolators. It is observed that failure occurs in the masonry elements only due to strain exceeding the limit value. The moderate, extensive, and collapsed damage states are indicated in the pushover curves by the marker. The damage states and corresponding displacement capacities are estimated based on the inter-story drift criteria, as presented in Fig. 9. The inter-story drift and damage in the upper story are more significant than that in the lower story. Figure 13 shows the displacement capacity at different damage states. The horizontal axis of the plot indicates the displacement component for loading. It was found that the displacement capacity of the U-STRP base-isolated building is significantly higher than that of the non-isolated building. The capacity of non-isolated buildings for different loadings is comparable. The displacement capacity in a U-STRP base-isolated building is substantially higher in the strong axis than that of the weak axis. The DBI building has a higher capacity than that of the SBI building in the strong axis, and the capacities of both buildings are comparable in the weak axis. In non-isolated buildings, moderate, extensive, and collapsed damage occur at the top

floor displacement of about 5 mm, 15 mm, and 20.0 mm, respectively. Base isolation significantly delays these damage states with respect to the floor displacement, and the DBI system shows superior performance to the SBI system. At the moderate damage state, the displacement capacity of the base-isolated building is 55–75 mm for X directional loading, whereas 40–49 mm for Y directional and 45° loadings. In an extensive damage state, the displacement capacity in the X direction is 132–148 mm and 78–98 for load in the Y and 45° directions. At the collapse level, the displacement capacity in the strong axis is 215–240 mm, and it is 114–140 in the weak direction and 45° directions.

Therefore, a U-STRP base isolation is efficient in mitigating the seismic vulnerability of masonry buildings in terms of damage state delaying. The shear strain in the isolator is denoted γ in the pushover curves, which indicates that the shear strain in the DBI system is higher than that of the SBI. The maximum shear strain in the strong and weaker axes is 215% and 114%, respectively, in the SBI system. The same is 240% and 114% in the DBI building. Due to the 45° orientation of the loading, the maximum shear strain in the X and Y directions is 129% and 91% in the SBI building. In the DBI building, it is 140% and 125%. It is found that the U-STRP base isolated building reaches the damage state DS5 only

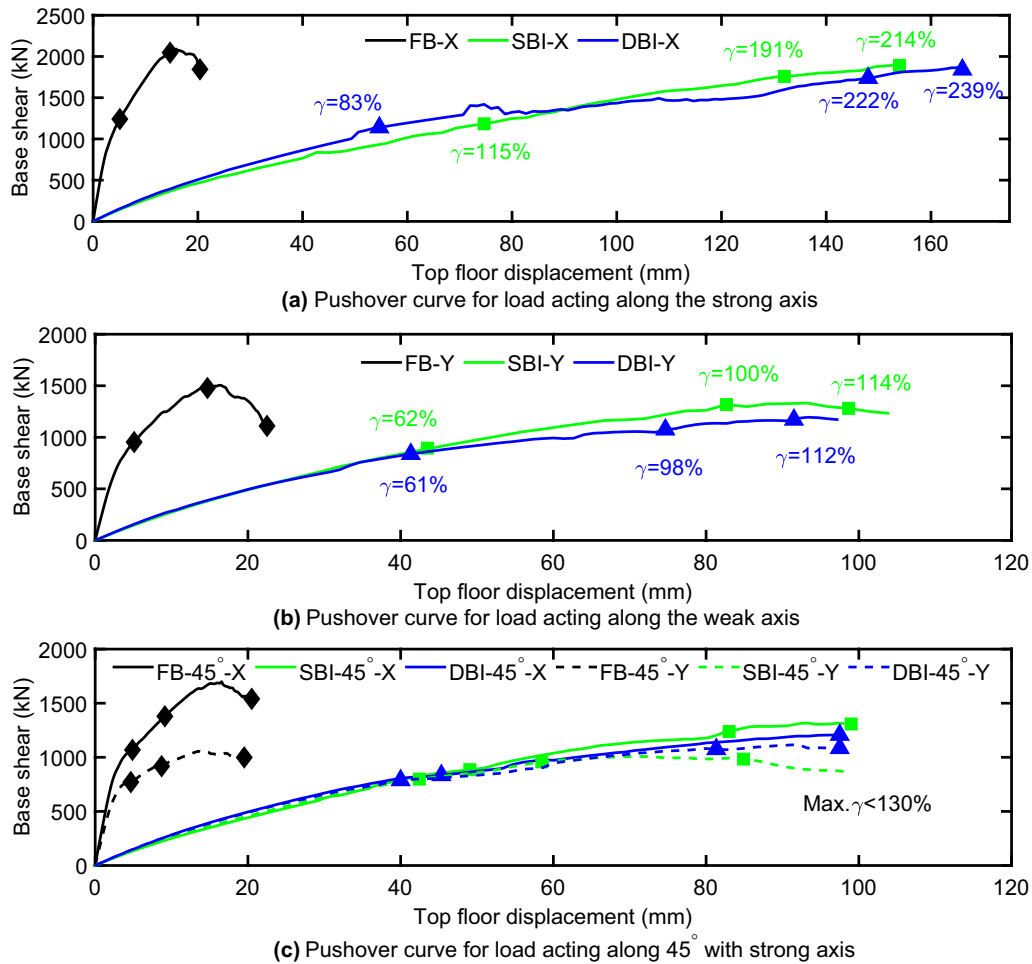


Fig. 12 Pushover curve of base-isolated and non-isolated masonry buildings

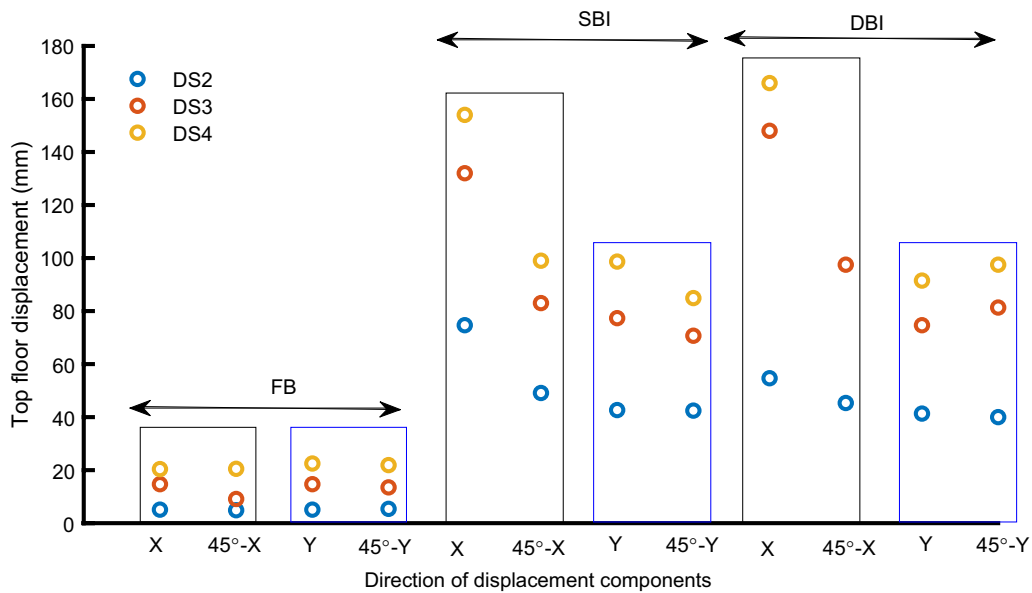


Fig. 13 Displacement capacity of different masonry buildings at different damage states

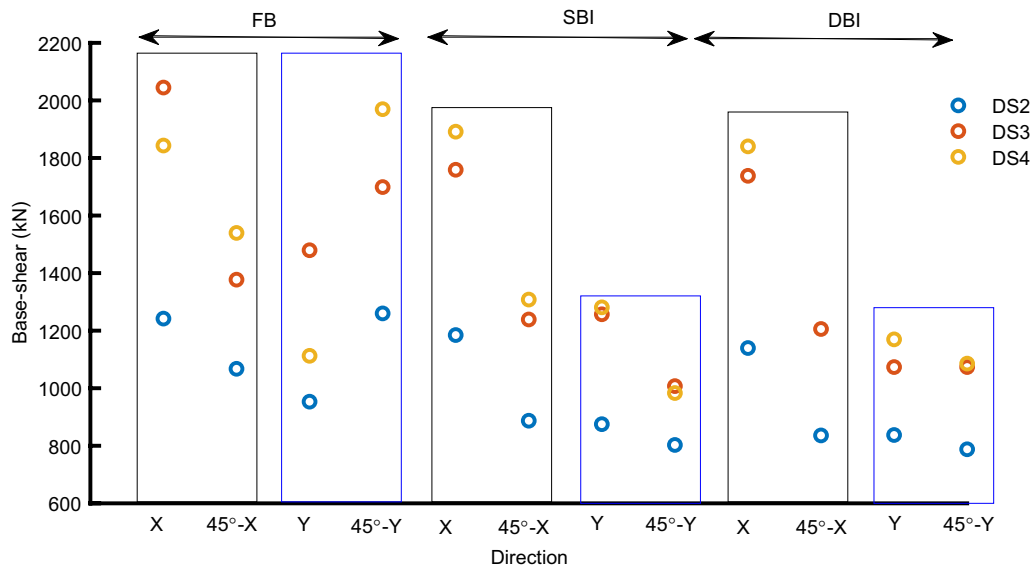


Fig. 14 Base shear in different masonry buildings at different damage states

when the load is acting in the X-direction because of the low aspect ratio of the isolator.

Figure 14 shows the base shear capacity of masonry buildings at different damage states. The base shear capacity in a U-STRP base-isolated building is lower than that of a fixed-base building. Until damage state DS2, the base-shears in DBI and SBI buildings are comparable. Then, at damage states DS3 and DS4, base shear in the SBI building is slightly higher than that of the DBI building.

Fragility analysis of masonry buildings

The fragility curve generated from the pushover analysis is a popular method used in the seismic vulnerability assessment of buildings (El-Maissi et al., 2022; Kassem et al., 2019; Nazri et al., 2018). The fragility curve is a cumulative lognormal probability distribution function that graphically represents the probability of reaching or exceeding a given damage state for a given intensity measure (spectral displacement or inter-story drift). At a given spectral displacement S_d , the conditional probability of being in or exceeding a particular damage state, DS, as per HAZUS (FEMA, 2003; Nazri et al., 2018; El-Maissi et al., 2022), is as follows:

$$P[DS|S_d] = \Phi \left[\frac{1}{\beta_{DS}} \ln \left(\frac{S_d}{\bar{S}_{d,DS}} \right) \right], \tag{8}$$

where $\bar{S}_{d,DS}$ is the median value of the lognormal distribution of the spectral displacement that produces the damage state threshold. The value of $\bar{S}_{d,DS}$ at different damage states found from the pushover curves are listed in Table 6. The median of spectral displacement $\bar{S}_{d,DS}$ for a damaged state is the displacement corresponding to 50% of the type of building that would reach or exceed the damage state. Φ is the standard normal cumulative distribution function. β_{DS} is the standard deviation of the natural logarithm of spectral displacement of the damage state, DS. The dispersion β_{DS} depends on the uncertainties in the seismic demand, such as the derivation of the hazard curve, the variability of the seismic intensity, the uncertain definition of the limit state threshold, and the variability of the capacity of buildings. A value of β_{DS} (ATC-58, 2012; FEMA, 2003; Thuyet et al., 2018) is 0.65 for the low-rise building that is used for the current study. These codes suggest a value of 0.75, 0.70, and 0.65 for buildings designed to old, moderate, and modern codes, respectively. The spectral displacement S_d is the

Table 6 Median of spectral displacement $\bar{S}_{d,DS}$ (mm) at different damage states

Damage state	FB system				SBI system				DBI system			
	X	Y	45°-X	45°-Y	X	Y	45°-X	45°-Y	X	Y	45°-X	45°-Y
DS2	2.6	2.6	2.4	2.3	37.3	21.3	24.5	21.7	27.3	20.7	22.7	20.0
DS3	9.9	9.9	7.0	6.7	102.7	60.0	66.5	50.9	101.3	58.0	71.3	60.7
DS4	17.6	18.6	14.4	14.1	142.7	88.0	91.0	71.7	157.3	82.7	–	89.3

displacement capacity as given in the pushover curve. The capacity spectrum in acceleration–displacement (AD) format is obtained by dividing the shear force in the pushover diagram by the seismic weight.

$$S_a = \frac{V}{W}, \tag{9}$$

where S_a is the spectral acceleration, V is the base shear, and W is the seismic weight. The seismic demand of masonry buildings in AD format is derived from the traditional elastic acceleration spectrum, S_{ae} , in which spectral acceleration is expressed in terms of the period using the following equation.

$$S_{de} = \frac{T^2}{4\pi^2} S_{ae}. \tag{10}$$

here S_{de} is the elastic displacement spectrum corresponding to period T and fixed viscous damping. Figure 15 shows the capacity spectrum and demand spectrum of masonry

buildings in AD format. The demand spectrum is the 5% damped elastic response spectrum at the seismic site class of D , such as $S_S = 0.25$ and $S_1 = 0.10$, as specified in ASCE/SEI 7-10. Here, S_S and S_1 mean mapped spectral response acceleration parameters at short and 1 s periods, respectively. According to Fig. 15, the seismic demand of the masonry building is around 30 mm for the assumed site.

Figure 16 shows the comparison of the fragility curves for the fixed-base and base-isolated masonry buildings. The comparison shows that the seismic vulnerability of the U-STRP base-isolated building for a spectral displacement is substantially lower than that of the fixed base building. Again, for a fixed spectral displacement, the seismic vulnerability along the strong axis, as shown in Fig. 16a, is considerably lower than that of the weak axis, as shown in Fig. 16b. The lower stiffness of masonry buildings yields high lateral drift, and masonry buildings fail due to exceedance of the strain limit. Besides, isolators in SBI systems are aligned parallel to the weak axis of the building to increase the rigidity. Therefore, the lower aspect

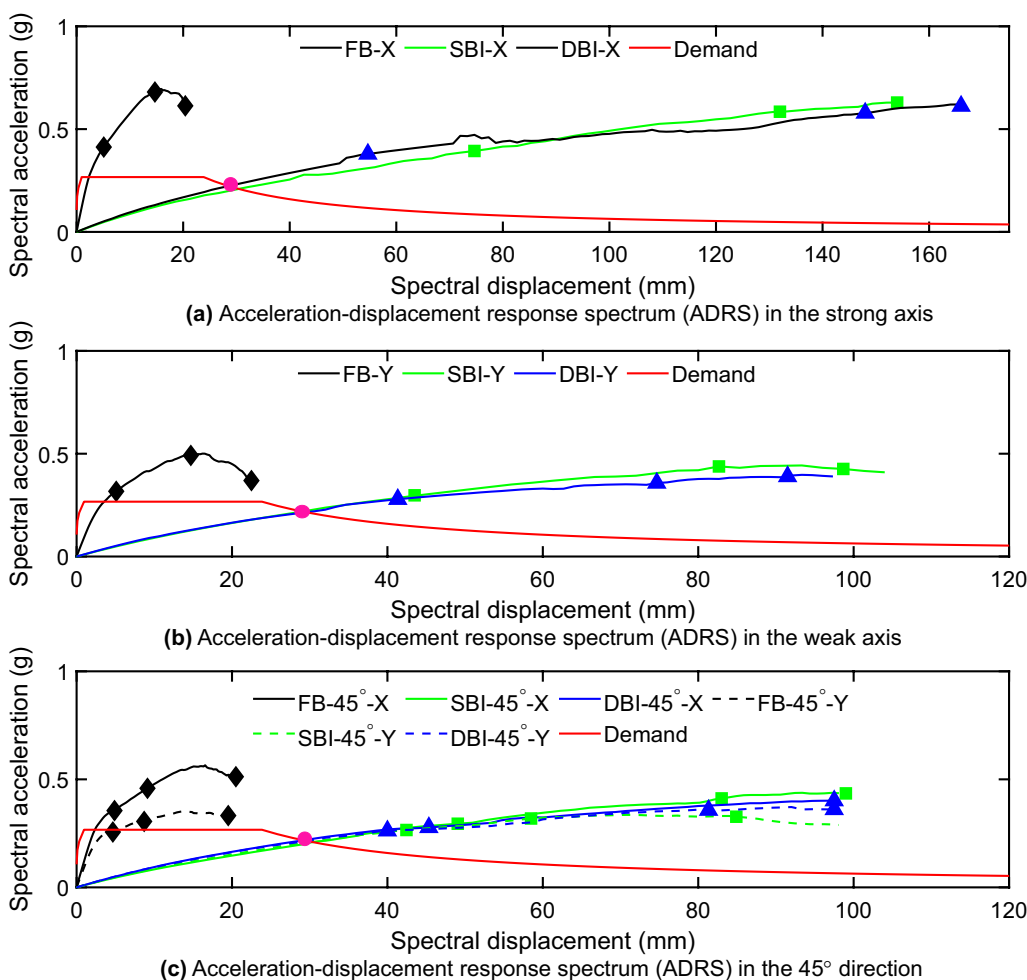


Fig. 15 Acceleration–displacement response spectrum (ADRS) of fixed base and base-isolated building

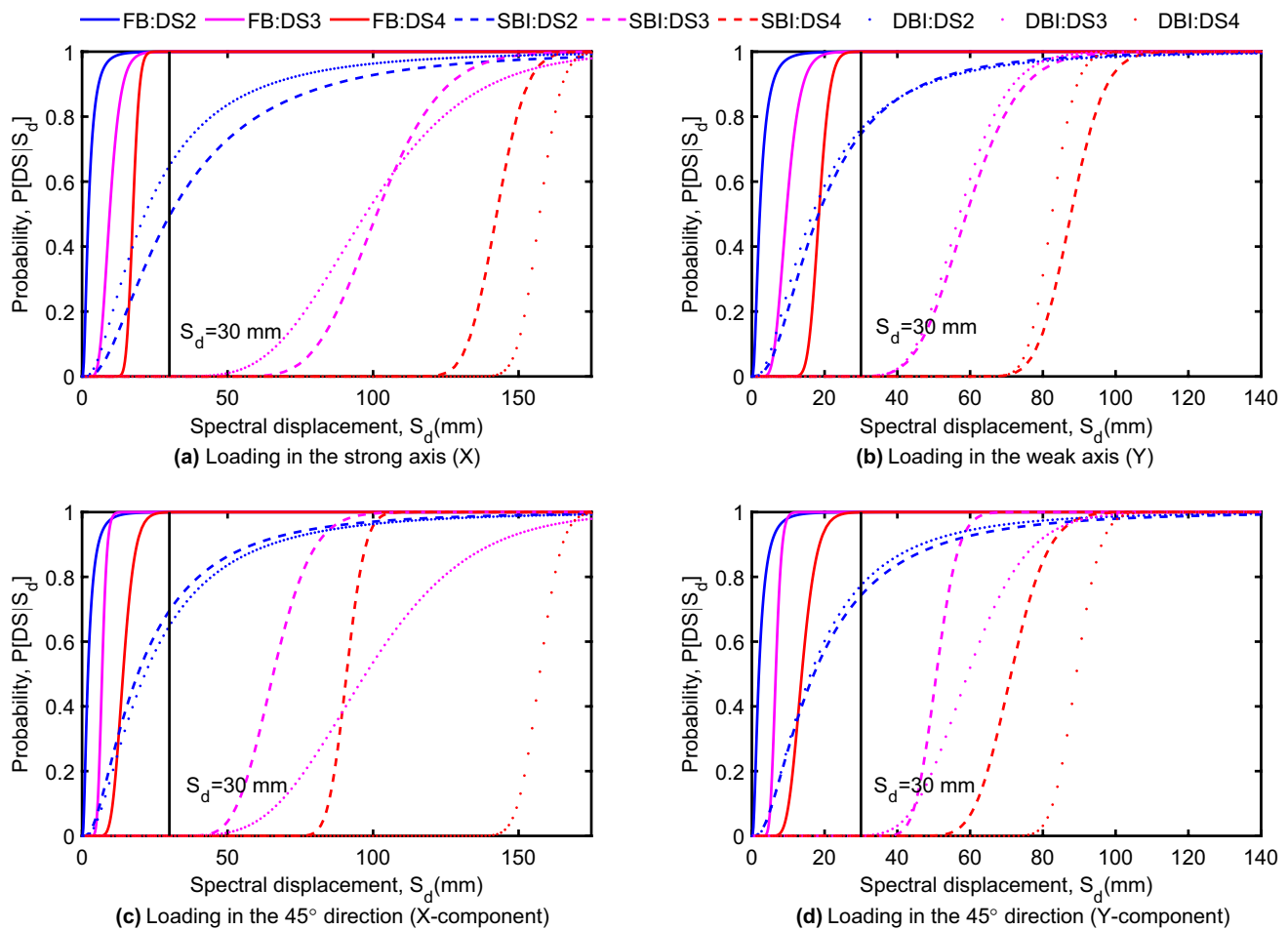


Fig. 16 Comparison of fragility curves of fixed base and base-isolated building

ratio of the strip-shaped isolator and the higher stiffness of the building in the strong axis reduce seismic vulnerability. The fragility curves also show that the 45° aligned displacement is more vulnerable than that of the displacement in the principal axis.

The seismic vulnerability of masonry buildings is figured out in site class D such that $S_S = 0.25$ and $S_I = 0.10$ to understand the efficiency of U-STRP isolation. The damage probability of different building systems at 30 mm spectral displacement is marked in the figures. The probability of exceedance for collapse damage, DS4 at 30 mm, is about 100% in the fixed base building, which indicates complete collapse in site class D such that $S_S = 0.25$ and $S_I = 0.10$. In the same seismicity, the probability of exceedance for moderate damage DS2 is 48% and 73% in the strong and weak axes of the SBI building, respectively. The probability of exceedance at the same damage state is 65% and 77% in the DBI building. For 45° aligned loading, the seismic vulnerability in SBI and DBI systems at moderate damage DS2 is comparable and falls in the range of 70–75% and 66–77%, respectively. The probability of exceedance for extensive and

collapsed damage states is about zero in the base-isolated buildings. Therefore, U-STRP base-isolation is efficient in reducing the seismic vulnerability of masonry buildings.

Conclusion

This paper focused on the performance and seismic vulnerability of masonry buildings supported by strip-shaped and uniformly distributed square-shaped U-STRP isolators. A two-story masonry building conventionally designed with material properties is modeled and analyzed. The structure is analyzed for loads acting along the principal axes and in the inclined direction (at an angle of 45° with the principal axis). The damage states of masonry buildings and their seismic vulnerability are determined based on inter-story drift and fragility analysis. From the analysis results, the following conclusions can be drawn:

- The U-STRP base-isolation mitigates the seismic vulnerability by delaying the damage occurrence. The displace-

ment capacity of the uniformly distributed square-shaped U-STRP base-isolated building is higher than that of the strip-shaped base-isolated building. The displacement capacity of the masonry building decreases when the load is applied at 45°.

- Lateral strain in the uniformly distributed square-shaped U-STRP isolator system is higher than that of the strip-shaped isolator system. The maximum strain exceeds 200% but remains below 250% even after the collapsed damage. The lateral strain for a 45° aligned load is substantially low. In the extensive and collapsed damage, the base shear in the strip-shaped isolator system is slightly higher than that of the uniformly distributed square-shaped U-STRP isolator system.
- Fragility curves of masonry buildings corresponding to different damage states indicate a significant reduction in the seismic vulnerability of the base isolated building as compared to that of the fixed base building.

Acknowledgements Akira Igarashi, Professor, DPRI, Kyoto University, Japan, who has launched the research on STRP isolator, is heartily acknowledged by the authors for his assistance and leadership. Additionally, the authors are grateful for the MSC Marc Mentat Software support which is provided by Akira Igarashi.

Author contributions Md.BZ organized the concept, performed the finite element analysis and wrote the paper. Md.NH organized the paper contains. Md.AH revised and checked the contents of the paper.

Funding This work was supported by the Ministry of Education, Culture, Sports, Science and Technology (MEXT) [MEXT Scholarship number: 183277].

Declarations

Conflict of interest On behalf of all authors, the corresponding author states that there is no conflict of interest.

References

- Applied Technology Council (ATC). (2012). *Seismic performance assessment of buildings, Volume 1—Methodology*, ATC-58, Redwood City, CA.
- Calabrese, A., Spizzuoco, M., Serino, G., Corte, G. D., & Maddaloni, G. (2015). Shaking table investigation of a novel, low-cost, base isolation technology using recycled rubber. *Structural Control and Health Monitoring*, 22(1), 107–122.
- Calvi, G. M. (1999). A displacement-based approach for vulnerability evaluation of classes of buildings. *Journal of Earthquake Engineering*, 3(3), 411–438.
- Choudhury, T., Milani, G., & Kaushik, H. B. (2015). Comprehensive numerical approaches for the design and safety assessment of masonry buildings retrofitted with steel bands in developing countries: the case of India. *Construction and Building Materials*, 85, 227–246.
- Costello, G. A. (1997). *Theory of wire rope* (2nd ed.). New York, USA: Springer-Verlag.
- Crisfield, M. A. (1982). Variable step lengths for nonlinear structural analysis, Report 1049, Transport and Road Research Lab., Crowthorne, England.
- El-Maissi, A. M., Kassem, M. M., Tan, C. G., et al. (2022). Damage index seismic assessment methodologies of URM buildings: a state-of-the-art review. *Engineering Journal*, 26(1), 39–53.
- Eurocode 8. (2004). Design of structures for earthquake resistance, BS EN 1998-1:2004.
- FEMA-443. (2003). *HAZUS-MH technical manual*. Washington, DC: Federal Emergency Management Agency.
- Feng, Y., Yi, D., & Bi, Q. (2011). Seismic design analysis of the country masonry school buildings in the meizoseismal area. *Earthquake Engineering and Engineering Vibration*, 10, 359–367.
- Habieb, A. B., Milani, G., Tavio, T., & Milani, F. (2017). Numerical model of low cost rubber isolators for masonry housing in high seismic regions. *International Journal of Civil and Environmental Engineering*, 11(5), 664–670.
- Hadad, H. A., Calabrese, A., Strano, S., & Serino, G. (2017). A base isolation system for developing countries using discarded tyres filled with elastomeric recycled materials. *Journal of Earthquake Engineering*, 21(2), 246–266.
- Jain, S. C., & Kennedy, J. B. (1974). Yield criterion for reinforced concrete slabs. *Journal of the Structural Division*, 100(3), 631–644.
- Kassem, M. M., Mohamed Nazri, F., Wei, L. J., et al. (2019). Seismic fragility assessment for moment-resisting concrete frame with setback under repeated earthquakes. *Asian Journal of Civil Engineering*, 20, 465–477.
- Kelly, M. J. (2002). Seismic isolation systems for developing countries. *EERI Distinguished Lecture, Earthquake Spectra*, 18(3), 385–406.
- Li, L. (1984). Base isolation measure for aseismic buildings in China. In *Proceedings of the 8th World conference on earthquake engineering*, 1984.
- Losanno, D., Spizzuoco, M., & Calabrese, A. (2019). Bidirectional shaking-table tests of unbonded recycled-rubber fiber-reinforced bearings (RR-FRBs). *Struct Control Health Monitoring*, 26(9), e2386.
- Maddaloni, G., Caterino, N., & Occhiuzzi, A. (2017). Shake table investigation of a structure isolated by recycled rubber devices and magnetorheological dampers. *Structural Control Health Monitoring*, 24(5), 1906.
- Marc, M. S. C. (2020A). *Theory and user information* (Vol. A). MSC Software Corporation.
- May, P.J. (2002). Barriers to adoption and implementation of PBEE innovations, PEER Report 2002/20, Pacific Earthquake Engineering Research Center, University of California, Berkeley.
- Milani, G., Shehu, R., & Valente, M. (2017). Possibilities and limitations of innovative retrofitting for masonry churches: Advanced computations on three case studies. *Construction and Building Materials*, 147, 239–263.
- Milani, G., Shehu, R., & Valente, M. (2018). A kinematic limit analysis approach for seismic retrofitting of masonry towers through steel tie-rods. *Engineering Structures*, 160, 212–228.
- Mishra, H. K. (2012). Experimental and analytical studies on scrap tire rubber pads for application to seismic isolation of structures. Ph.D. thesis, Kyoto University, Kyoto, Japan.
- Mishra, H. K., & Igarashi, A. (2013). Lateral deformation capacity and stability of layer-bonded scrap tire rubber pad isolators under combined compressive and shear loading. *Structural Engineering and Mechanics*, 48(4), 479–500.
- Mishra, H. K., Igarashi, A., Ji, D., & Matsushima, H. (2014). Pseudodynamic testing for seismic performance assessment of buildings with seismic isolation system using scrap tire rubber pad isolators. *Journal of Civil Engineering and Architecture*, 8(1), 73–88.
- Mishra, H. K., Igarashi, A., & Matsushima, H. (2013). Finite element analysis and experimental verification of the scrap tire rubber pad isolator. *Bulletin Earthquake Engineering*, 11(2), 687–707.

- Morales, E., Filiatrault, A., & Aref, A. (2018). Seismic floor isolation using recycled tires for essential buildings in developing countries. *Bulletin of Earthquake Engineering*, 16, 6299–6333.
- Murtyl, C. V. R., Dutta, J., & Agrawal, S. K. (2004). Twin lintel belt in steel for seismic strengthening of brick masonry buildings. *Earthquake Engineering and Engineering Vibration*, 3, 215–222.
- Nanda, R. P., Shrikhande, M., & Agarwal, P. (2015). Low-cost base-isolation system for seismic protection of rural buildings. *Practice Periodical on Structural Design and Construction*, 21, 04015001.
- Nazri, F. M., Yerna, C. K., Kassema, M. M., & Farsangi, E. N. (2018). Assessment of structure-specific fragility curves for soft storey buildings implementing IDA and SPO approaches. *International Journal of Engineering*, 31(12), 2016–2021.
- Pan, P., Zamfirescu, D., Nakashima, N., Nakayasu, N., & Kashiwa, H. (2005). Base-isolation design practice in Japan: Introduction to the post-Kobe approach. *Journal of Earthquake Engineering*, 9(1), 147–171.
- Qamaruddin, M., Arya Rasheeduzzafar, S. A., & Chandra, B. (1986). Seismic response of masonry buildings with sliding substructure. *Journal of the Structural Engineering. American Society of Civil Engineers*, 112, 2001–2011.
- Spizzuoco, M., Calabrese, A., & Serino, G. (2014). Innovative low-cost recycled rubber-fiber reinforced isolator: experimental tests and finite element analyses. *Engineering Structures*, 76(1), 99–111.
- Thuyet, V. N., Deb, S. K., & Dutta, A. (2018). Mitigation of seismic vulnerability of prototype low-rise masonry building using U-FREIs. *Journal of Performance of Constructed Facilities*, 32(2), 04017136:1–13.
- Tsai, H.-C., & Kelly, J. M. (2002). Stiffness analysis of fiber-reinforced rectangular seismic isolators. *Journal of Engineering Mechanics, ASCE*, 128(4), 462–470.
- Turer, A., & Özden, B. (2008). Seismic base isolation using low-cost scrap tire pads (STP). *Materials and Structures*, 41(5), 891–908.
- Van Engelen, N. C., Konstantinidis, D., & Tait, M. J. (2016). Structural and nonstructural performance of a seismically isolated building using stable unbonded fiber-reinforced elastomeric isolators. *Earthquake Engineering and Structural Dynamics*, 45, 421–439.
- Zisan M. B., & Igarashi A. (2020). Lateral load performance evaluation of unbonded strip-STRP base isolator. In *17th World conference on earthquake engineering (17WCEE), September 13th to 18th, 2020, Sendai, Japan*.
- Zisan, M. B., & Igarashi, A. (2021). Lateral load performance and seismic demand of unbonded STRP base isolator. *Earthquake Engineering and Engineering Vibration*, 20, 803–821.

Publisher's Note Springer Nature remains neutral with regard to jurisdictional claims in published maps and institutional affiliations.

Springer Nature or its licensor holds exclusive rights to this article under a publishing agreement with the author(s) or other rightsholder(s); author self-archiving of the accepted manuscript version of this article is solely governed by the terms of such publishing agreement and applicable law.